Natural organic matter flocculation behavior controls lead phosphate particle aggregation by mono- and divalent cations

Juntao Zhao[1], Riya A. Mathew[1], David S. Yang[2], Peter G. Vekilov[2], Yandi Hu[1,3,4], and Stacey M. Louie[1]*

[1]Department of Civil & Environmental Engineering, University of Houston, Houston, TX 77004, USA

[2]Department of Chemical and Biomolecular Engineering, University of Houston, Houston, TX 77004, USA

[3]College of Environmental Sciences and Engineering, Peking University, Beijing, China, 100871

[4]State Environmental Protection Key Laboratory of All Material Fluxes in River Ecosystems, Beijing, China, 100871

*** Corresponding Author:**

E-mail: slouie@uh.edu

Phone: (713)743-8646

Submitted to ***Science of the Total Environment***

Abstract

Phosphate addition is commonly applied as an effective method to remediate lead contaminated sites via the formation of lead phosphate with low solubility. ~~However,~~ T~~t~~he effects of natural organic matter (NOM)~~) on the particle aggregation~~ and the potential influence of the molecular weight and chemistry of the NOM on the particle aggregation, however, are not ~~yet~~ currentlywell understood. This study investigates the influence of two aquatic NOM and two soil or coal humic acid (HA) extracts on the aggregation behavior of lead phosphate particles and explores the controlling mechanisms. All types of NOM induced disaggregation and steric stabilization of the particles in the presence of Na^{+} or low (1 mM) Ca^{2+} concentrations, as well as at low NOM concentrations (1 mg_C/L). However, for the soil and coal HA, a threshold at NOM concentrations of 10 mg_C/L and high (3 mM) Ca^{2+} concentrations was observed where bridging flocculation (rather than steric stabilization) occurred ~~at NOM concentrations of 10 mgC/L and high (3 mM) Ca2+ concentrations~~. *In situ* attenuated total reflectance – Fourier transform infrared ~~experiments~~ characterization confirmed adsorption of the soil and coal humic acid extracts (10 mg_C/L) onto the surface of the lead phosphate particles in 3 mM Ca^{2+}, ~~while~~ whereas dynamic and static light scattering demonstrated extensive HA flocculation that dominated the overall scattered light intensities. These results imply that the accelerated aggregation was induced by a combination of HA adsorption and bridging flocculation by Ca^{2+}. Overall, this research demonstrates that the type of NOM is critical to predict the colloidal stability of lead phosphate particles, with aquatic NOM stabilizing the particles under all conditions evaluated but soil or coal HA showing highly variable stabilization or flocculation behavior depending on the HA and Ca^{2+} concentrations. These results highlight the importance

of characterizing both the NOM and background electrolytes to better predict lead particle transport and exposure risks in applications of phosphate for lead remediation.

1. Introduction

Lead contamination is commonly observed in soils or waters that have historically been impacted by lead sources. As a result, elevated blood lead levels have been reported worldwide (Deshommes et al., 2018; Hanna-Attisha et al., 2016; Wu et al., 2020), which can induce severe health impacts, particularly in children (Zhang et al., 2012). To mitigate lead transport into water supplies and hence ~~exposure and~~its bioavailability, phosphate addition has been proposed as an effective method to immobilize lead via the formation of lead phosphates with low solubility (Ruby et al., 1994). In environmental engineering applications, phosphate species such as apatite have been widely used to immobilize Pb in lead contaminated sites (Guo et al., 2019; Ma et al., 1993; Mavropoulos et al., 2002). Mavropoulos et al. conducted batch experiments to test sorption of Pb by synthetic hydroxyapatite (HAP). They found an unstable solid solution, $Pb_{(10-x)}Ca_x(PO_4)_6(OH)_2$ (PbCaHAP), formed, and eventually it transformed to pure hydroxylpyromorphite ($Pb_{10}(PO_4)_6(OH)_2$) (Mavropoulos et al., 2002). ~~However, ~~I~~i~~f the lead phosphate particles are mobile in water, however, the phosphate treatment would not be effective in mitigating lead transport. Hence, the colloidal stability of the lead phosphate is important to ~~characterize to~~ better predict treatment efficiency.

Natural organic matter (NOM) is commonly present~~ed~~ in both aquatic environments and soils and is well known to affect the aggregation behavior of nanoparticles and colloids. To date, studies on NOM impacts on lead immobilization have been carried out primarily in whole soils or have investigated the effects of small organic acids as model compounds. Guo et al. compared the reduction of Pb availability in three types of soils with different pH treated with bioapatite in the presence and absence of oxalic acid, and found that oxalic acid facilitated the remediation by increasing the solubility of apatite for lead phosphate formation and that soil with neutral pH was the most suitable type for this remediation (Guo et al., 2019). Wei et al. reported a similar observation for oxalic acid. In addition, they observed that the presence of malic and citric acids inhibited the immobilization of Pb by apatite materials due to the formation of Pb-organic complexes (Wei et al., 2014). Landrot and Khaokaew fractionated soils by size and measured the speciation of Pb in each fraction. They found that in fine particles Pb-humate ~~in fine particles~~ was the highest, ~~while~~ whereas it was undetected in bulk soil (Landrot and Khaokaew, 2018). Our prior study showed that a coal-derived humic acid enhanced the colloidal stability and transport of lead phosphate particles in column deposition experiments in the presence of 0.2 mM Ca^{2+} (Zhao et al., 2022, 2018). Together, these studies suggest that NOM interactions can be especially important for lead-containing colloids that may pose a higher transport risk from soils, and that different compositions of organic matter can either enhance or diminish the immobilization efficiency by phosphate remediation.

A more systematic understanding of the effect of organic matter extracts from various natural sources on the colloidal stability of the lead phosphate particles would be beneficial to better predict their fate and transport under a broader range of environmental conditions. NOM properties that could influence the colloidal stability of the particles include the functional group composition (for example, carboxyl, amine, and thiol groups can participate in metal complexation or attachment of the NOM onto particle surfaces (Bala et al., 2007; Deonarine and Hsu-Kim, 2009; Jalilehvand et al., 2015)) and the molecular weight of the NOM. For example, Deonarine et al. observed that the aggregation rate of ZnS nanoparticles decreased with increasing aromatic carbon content in NOM (Deonarine et al., 2011), and Louie et al. found that the high molecular weight fraction of various types of NOM imparted greater colloidal stability than lower molecular weight fractions for Au nanoparticles in monovalent electrolytes (Louie et al., 2015a, 2013). In contrast, Vindedahl et al. found that fulvic acids were more efficient in hindering goethite aggregation than humic acids, as fulvic acids have a higher charge density (Vindedahl et al., 2016). Further variability is observed when comparing aggregation in monovalent or divalent cations. Shen et al. reported that the high molecular weight fractions of Suwannee River NOM stabilized nC_{60} nanoparticles in monovalent electrolyte, but they promoted nC_{60} aggregation in high concentrations of divalent electrolytes because of bridging flocculation by Ca^{2+} or Mg^{2+} (Shen et al., 2015). Huangfu et al. also observed that the aggregation of MnO_2 was facilitated due to bridging of high molecular weight alginate-Ca^{2+} complexes in > 5 mM Ca^{2+} (Huangfu et al., 2013). It is noted that Ca^{2+} can induce flocculation of NOM itself (without particles) via charge screening and bridging effects (Kloster et al., 2013). However, prior studies on particle aggregation did not specifically distinguish the roles of particle-particle attachment, NOM-NOM attachment, and NOM-particle attachment in the overall aggregation process in systems where bridging flocculation was observed.

The main objective of this study is to compare the effects of well-characterized reference NOM extracts from various sources (two aquatic NOMs, and two soil- or coal-derived humic acids) to identify key NOM properties and processes that control the colloidal stability of lead phosphate particles. Aggregation experiments of lead phosphate particles were carried out in the presence and absence of NOM and monovalent (Na^{+}) or divalent (Ca^{2+}) cations. In addition to investigating the size and zeta potential of the particles, ultraviolet–visible (UV-Vis) spectroscopy and size exclusion chromatography (SEC) were ~~utilized~~ employed to assess the molecular weight of the NOM, and the aggregation behavior of the NOM itself in the various background electrolytes was also evaluated. To investigate the various interactions of NOM with the lead phosphate particles, *in situ* attenuated total reflectance – Fourier transform infrared

(ATR-FTIR) spectroscopy was used to measure NOM adsorption, inductively coupled plasma mass spectroscopy (ICP-MS) was used to evaluate lead dissolution, and static light scattering (SLS) was used to evaluate the structure of particle or NOM flocs. This thorough characterization shed light on ~~enabled~~ the mechanisms involved in the particle-NOM~~ interactions to be elucidated~~, including adsorption of NOM onto the lead phosphate particles, particle dissagglomeration or dissolution by NOM, and colloidal stabilization or flocculation induced by NOM. This knowledge can contribute to an improved understanding of how the effectiveness of phosphate remediation of lead-contaminated sites depends on the environmental conditions.

2. Experimental Section

2.1. Precipitation and characterization of lead phosphate suspensions

Stock solutions of 10 mM $Pb(NO_3)_2$ (ACS reagent, ≥ 99.0%, Sigma-Aldrich, St. Louis, MO), 100 mM Na_2HPO_4 (99+ %, Acros Organics, Morris Plains, NJ), 100 mM NaH_2PO_4 (99%, Acros Organics, Morris Plains, NJ), and 1 M $NaNO_3$ (ACS reagent, ≥ 99.0%, Sigma-Aldrich, St Louis, MO) were prepared using aerated ultrapure water (resistivity > 18 mΩ). The stock solutions were used to precipitate lead phosphate particles (Table S1). In detail, 70 μL of 100 mM Na_2HPO_4, 80 μL of 100 mM NaH_2PO_4, 45 μL of 1 M $NaNO_3$, and 14.655 mL of ultrapure water were mixed well in a 15 mL centrifuge tube; then, 150 μL of 10 mM $Pb(NO_3)_2$ was added to start the precipitation. The mixture was vortexed for 5 s immediately after the addition of $Pb(NO_3)_2$. The synthesized particles were characterized by DLS for the *z*-average diameter using a cumulants fit (Zetasizer Nano ZS, Malvern Panalytical, Malvern, UK). Zeta potential was measured using a dip cell (ZEN1002, Malvern Panalytical, Malvern, UK) with voltage set to 5

V and using the Smoluchowski model to convert electrophoretic mobility to apparent zeta potential.

2.2. Preparation and characterization of NOM stock solutions

Four types of NOM were purchased from the International Humic Substances Society (IHSS, St. Paul, MN) that encompass a range of properties (molecular weight and functional group compositions): Upper Mississippi River NOM (UMRNOM, cat. no. 1R110N), Suwannee River NOM (SRNOM, 2R101N), Pahokee Peat humic acid (PPHA, 1S103H), and Leonardite humic acid (LHA, 1S104H). Tables S2 and S3 show the properties of the selected NOM reported by the IHSS, including their elemental compositions and functional group distributions (International Humic Substances Society (IHSS), 2022). According to the different isolation methods used to extract these NOM, the aquatic UMRNOM and SRNOM are expected to contain more hydrophilic, lower molecular weight species, whereas PPHA and LHA contain more hydrophobic, higher molecular weight species (Thurman, 1985). Indeed, carboxyl density increase from LHA to PPHA to SRNOM to UMRNOM (Table S2), while aromaticity increases following the opposite sequence (Table S3). For S content, UMRNOM > SRNOM > LHA > PPHA, and for N content, PPHA > UMRNOM > SRNOM > LHA.

Stock solutions of the four types of NOM were prepared. Glass total organic carbon (TOC) vials were cleaned, heated in a furnace at 550°C for 2 h to remove any organic matter residues, and cooled at room temperature for preparation of all NOM stocks and TOC analysis. For each NOM type, 20 mg of NOM was added to a clean glass vial along with 20 mL of ultrapure water, the pH of the NOM solution was adjusted to 7 using 1 M and 0.1 M NaOH, and the NOM solution was rotated end-over-end overnight to dissolve. After rotation, the solutions were filtered through 0.22 μm polyethersulfone (PES) membrane filters (EMD Millipore, Burlington, MA), and the filtrate was diluted and measured using a TOC analyzer (TOC-L, Shimadzu, Columbia, MD) to obtain the C concentration in the filtered stocks.

UV-Vis absorbance spectra were collected on a spectrophotometer (UV-2600, Shimadzu, Columbia, MD) on the four NOM samples at 10 mg_C/L in ultrapure water. The spectra were collected in a quartz cuvette across a wavelength range from 800 nm to 200 nm. The percentage of aromatic functional groups was estimated using previously reported correlation equations by Abbt-Braun et al. and Chin et al. based on the specific UV absorbance at 254 nm and 280 nm, respectively (Abbt-Braun et al., 2004; Chin et al., 1994). The spectra were also fitted by an exponential model to determine the slope coefficient (S), which is inversely related to molecular weight (Equation 1) (Bricaud et al., 1981):

$$A_\lambda = A_{\lambda_0} \exp\left[-S(\lambda - \lambda_0)\right] \tag{1}$$

where A_λ is the absorbance at wavelength λ, and A_{λ_0} is the absorbance at a reference wavelength λ_0 (450 nm here). This analysis allows for qualitative comparison of the molecular weights of the four types of NOM.

To quantitatively estimate molecular weights and investigate the molecular weight distribution of the NOM, the filtered NOM stocks (nominal 1 g/L) were characterized by size exclusion chromatography (SEC). All samples were analyzed on an Agilent 1290 Infinity liquid chromatography system (Agilent Technologies, Santa Clara, CA) using a 100 μL injection volume onto a Superdex 75 10/300 GL analytical SEC column (GE Healthcare, Piscataway, NJ), followed by a UV-Vis diode array detector (Agilent 1260 Infinity, Agilent Technologies, Santa Clara, CA), multi-angle light scattering (MALS) detector (HELEOS II, Wyatt Technology, Santa Barbara, CA), and differential refractive index (dRI) detector (Optilab T-rEX, Wyatt Technology, Santa Barbara, CA). The mobile phase was 4 mM phosphate (pH 7) with 25 mM NaCl, and the flow rate was 0.5 mL/min. The UV-Vis detector was set to monitor the 280 nm wavelength. Molecular weight was estimated on the NOM samples using the dRI detector for concentration with Zimm analysis on the MALS data collected at 10 scattering angles from 37.5° to 120.1°. The refractive index increment, d*n*/d*c*, is required to determine mass concentration from the dRI signal. Measured values of 0.146 mL/g for SRNOM (Shakiba et al., 2018) and 0.27 mL/g for PPHA (Louie et al., 2015b) were determined in our prior studies. The d*n*/d*c* for UMRNOM and LHA were determined in this study by batch syringe injection of six calibration solutions (from 5 mg/L to 100 mg/L total mass) diluted in ultrapure water from a 1 g/L unfiltered stock solution (prepared in ultrapure water and adjusted to pH 7 with NaOH), which yielded calibration slopes (d*n*/d*c*) of 0.212 mL/g and 0.250 mL/g for UMRNOM and LHA, respectively.

2.3. Lead phosphate and NOM aggregation experiments

To characterize the aggregation behavior of lead phosphate particles in the presence of NOM and different electrolytes, time-resolved DLS measurements were conducted. All samples were ~~prepared~~ diluted to a total volume of 1 mL in a DLS cuvette (ZEN0040, Malvern Instruments Ltd.) with a final mixture concentration of 1 mg/L (as Pb) of lead phosphate particles; (0, 1, or 10) mg as $_C$/L of NOM; and no added salts, 100 mM $NaNO_3$ or (1 or 3) mM of $Ca(NO_3)_2$ for the background electrolyte. These NOM concentrations were selected because they are within the typical dissolved organic carbon (DOC) concentration range in natural waters (0.5 to 30 mg$_C$/L) (Thurman, 1985). The electrolyte concentrations were selected because they are all above the CCC of the lead phosphate particles as measured in our prior studies (Zhao et al., 2022, 2018), which allows us to most clearly observe the influence of the NOM to either stabilize particles, i.e., change the CCC, or destabilize the particles by bridging, i.e., induce more rapid agglomeration than the "diffusion" limit (Abe et al., 2011; Chen and Elimelech, 2007; Ghosh et al., 2008; Liu et al., 2011; Tiller and O'Melia, 1993). The Ca^{2+} concentrations are also within the range previously reported for slow to fast aggregation of a humic acid (Kloster et al., 2013).

To minimize delay time between sample preparation and the start of the DLS data collection, the optimal attenuator and measurement position settings were determined by allowing the Zetasizer instrument to automatically optimize these settings on a sample of 1 mg/L (as Pb) of lead phosphate particles in DI water; then, the same settings were manually set for the time-resolved measurements. To prepare the sample mixtures, ultrapure water, NOM stock (for conditions with NOM), and lead phosphate suspension were first added to the DLS cuvette, vortexed for 5 s, and held for 15 min to allow NOM adsorption; the particle size was measured every 3 min. Then, $NaNO_3$ or $Ca(NO_3)_2$ stock solution (10 mM $Ca(NO_3)_2$ (from $Ca(NO_3)_2•4H_2O$, ACS reagent, 99+%, Acros Organics, Morris Plains, NJ) or 1 M $NaNO_3$ in ultrapure water) was added to achieve the desired concentration in the mixture. The final mixture was vortexed for 5 s, and the particle size was recorded every 15 s for 15 min continuously. For comparison, similar measurements were conducted on lead phosphate particles in the absence of NOM, as well as lead phosphate particles with or without NOM in ultrapure water without any additional salts (Ca^{2+} or Na^+). In addition, NOM-only controls were measured in all background electrolytes. At the end of the experiment, a dip cell (ZEN1002, Malvern Panalytical, Malvern, UK) was capped on the cuvette cell, and zeta potential was measured. Because agglomeration of the particles, PPHA, and LHA were observed in the presence of 3 mM Ca^{2+}, the CCC was also determined by conducting time-resolved DLS measurements at varied $Ca(NO_3)_2$ concentrations.

To better interpret the DLS results on samples where aggregation was observed, static light scattering (SLS) measurements were conducted on the lead phosphate particle suspensions in all of the background electrolytes without NOM, the PPHA or LHA (without lead phosphate) in 3 mM $Ca(NO_3)_2$, and the mixtures of particles with PPHA or LHA in 3 mM $Ca(NO_3)_2$. Details on the SLS measurements can be found in the Supporting Information (SI).

2.4. Lead dissolution experiments

Under several conditions, particularly 10 mg_C/L in 1 mM $Ca(NO_3)_2$, a decrease in particle size was observed in the aggregation experiments. To evaluate potential lead phosphate dissolution, additional experiments were performed to pellet the particles by centrifugation and quantify lead in the supernatant by inductively coupled plasma – mass spectrometry (ICP-MS). First, 2 mL of a mixture of lead phosphate particles (1 mg/L as Pb), 1 mM $Ca(NO_3)_2$, and 10 mg_C/L of NOM. Controls were also prepared of the lead phosphate particles in 1 mM $Ca(NO_3)_2$ without NOM. After holding the samples for 15 min (the duration of the aggregation measurements), the samples were then centrifuged at 13000 rpm (11337 *g*) for 15 min (MiniSpin Plus, Eppendorf, Enfield, CT), and 1.5 mL of supernatant was collected. Based on the sedimentation equation and given the rotor geometry, centrifugal force, and lead phosphate density of 7 g/cm^3, it is estimated that nanoparticles with diameters > 30 nm will settle from the top to the bottom of the centrifuge tube under the applied conditions. Control samples were also prepared that were not centrifuged, in order to confirm the total lead concentration. All samples were prepared for ICP-MS analysis by diluting the samples and acidifying to 2% nitric acid (TraceMetal grade, Fisher Scientific, Waltham, MA). The ICP-MS analysis for ^{208}Pb was conducted on an iCAP RQ quadrupole ICP-MS (ThermoFisher Scientific, Waltham, MA) against external calibration standards. The sample flow rate was 0.4 mL/min and dwell time was 10 ms.

2.5. Adsorption experiments

<u>2.5.1. UV-Vis spectroscopy</u>

To investigate adsorption of NOM onto the lead phosphate particles, adsorption experiments were performed in a laminar flow hood (Air Science, Fort Myers, FL). Stock solutions and ultrapure water were mixed in a 2 mL microcentrifuge tube to obtain a lead phosphate concentration of 10 mg/L (as Pb) and NOM concentration of 10 mg_C/L in either ultrapure water, 100 mM $NaNO_3$, or 1 mM or 3 mM $Ca(NO_3)_2$. It is noted that a higher particle concentration was selected compared to the aggregation experiments because the percent removal of NOM from solution by adsorption is expected to be low. The mixture was held for 15 min, and then centrifuged at 13000 rpm (11337 *g*) (Eppendorf, MiniSpin Plus, Enfield, CT, USA) for 15 min. Then, 1.8 mL of the supernatant was collected and measured by UV-Vis spectroscopy (UV-2600, Shimadzu, Columbia, MD). Control samples of NOM in the absence of lead phosphate particles, with and without centrifuging, were also measured.

2.5.2. *In situ* attenuated total reflectance – Fourier transform infrared (ATR-FTIR) spectroscopy

In situ ATR-FTIR measurements were also conducted to evaluate NOM adsorption onto the lead phosphate particles. The advantage of the *in situ* flow cell experiment is that adsorption of NOM to the particle surface is directly probed. In other, indirect methods that require particles to be removed by centrifugation or ultrafiltration to quantify depletion of the unadsorbed NOM in solution, large or dense NOM flocs or aggregates may be removed along with the particles; in addition, solution depletion measurements are not sensitive to small concentration changes if the adsorptive removal is low. In contrast, the *in situ* ATR measurements have a limited IR penetration depth beyond the ATR crystal and hence selectively investigate the particles deposited on the ATR crystal, rather than the bulk NOM solution. Settling deposition of NOM is also minimized by continuously flowing the solution over the particles during the experiment.

Experiments were conducted on a diamond/ZnSe single reflection ATR crystal equipped with a flow cell apparatus (PIKE Technologies, Fitchburg, WI), and FTIR spectra were collected on a Nicolet iS50 FTIR spectrometer (Thermo Fisher Scientific, Waltham, MA) from 800 cm^{-1} to 4000 cm^{-1} at 2 cm^{-1} resolution with 200 scans averaged per measurement. To prepare a concentrated particle suspension for deposition onto the ATR crystal, 2 mL of lead phosphate particle stock as-synthesized (20 mg/L as Pb) was pelleted by centrifugation at 13000 rpm (11337 *g*) for 15 min (Eppendorf, MiniSpin Plus, Enfield, CT, USA) and was further concentrated by two more additions and centrifugation of lead phosphate stock after removing supernatant. To remove excess phosphate in the solution, the concentrated particles were then washed three times by replacing the supernatant with ultrapure water, centrifuging, and removing supernatant. Based on mass balance calculations on measured masses at each centrifugation and dilution step, the final concentration of washed particles was (2.35 ± 0.03) g/L as Pb and the phosphate concentration was $(5.40 \pm 0.07) \times 10^{-6}$ mM. A volume of 6 μL of the washed, concentrated NPs was deposited and dried on ATR crystal. The spectrum of the dried lead phosphate particles was collected.

The flow cell apparatus was clamped over the diamond/ZnSe ATR crystal, and a syringe pump was used to continually inject solutions over the deposited lead phosphate particles at a flow rate of 2.43 mL/h (Razel R99-E, Saint Albans, VT, USA). First, background electrolyte solution (100 mM $NaNO_3$ or 3 mM $Ca(NO_3)_2$) was flowed over the dried particles for 15 min (collecting spectra every 5 min) to remove any loosely bound particles and collect a background spectrum of the particle surface equilibrated in the electrolyte solution. Next, a solution of 10 mg_C/L of NOM (PPHA, LHA, UMRNOM, or SRNOM) in background electrolyte (100 mM $NaNO_3$ or 3 mM $Ca(NO_3)_2$) was flowed for 35 min, collecting spectra every 5 min, to evaluate adsorption of NOM relative to the background spectrum. Finally, to evaluate any desorption of loosely adsorbed or deposited NOM, the same background electrolyte solution (without NOM) was flowed for 15 min; spectra were collected every 5 min and compared to the last spectrum from the NOM adsorption step. To normalize the spectra collected across all experiments for differences in the amount of lead phosphate particles deposited in the ATR measurement window, the phosphate peak heights were determined at 975 cm^{-1} on the dried particle spectrum collected for each experiment and used to scale the NOM adsorption and desorption spectra.

3. Results and Discussion

3.1. Characterization of the Lead Phosphate Particles and NOM Isolates

The *z*-average diameter of the lead phosphate particles formed in the precipitation solution (20.5 ± 0.7 mg/L as Pb) was 228 ± 4 nm (n = 4 independently synthesized samples), and the zeta potential was -39.6 ± 0.1 mV (Figure S1). From the TOC measurement results, the measured concentrations of the filtered NOM stock solutions (nominal 1 g/L total mass) were (0.36, 0.39, 0.43, and 0.39) g/L as C for UMRNOM, SRNOM, PPHA, and LHA respectively.

UV–vis absorbance spectra were collected on the NOM solutions (Figure 1(a)). Applying correlation equations relating aromaticity to the specific UV absorbance(Abbt-Braun et al., 2004; Chin et al., 1994) provides an estimated aromaticity of 26%, 28%, 51%, and 62%, for UMRNOM, SRNOM, PPHA, and LHA, respectively. The exponential slopes, S, of the spectra (Figure 1(b)) were similar for UMRNOM and SRNOM (0.0139 and 0.0135 nm^{-1}, respectively), which were higher than S for PPHA and LHA (0.0091 and 0.0089 nm^{-1}, respectively). Molecular weight is generally inversely correlated to S, so this analysis suggests that PPHA and LHA have higher molecular weights. These trends correspond with expectations for lower solubility soil- and coal-derived humic acids to have higher aromaticity and higher average molecular weights than aquatic NOM.

The SEC results are shown in Figure S2 for the molecular weight distribution analysis. The total recovery (by UV detection at 280 nm) of NOM from the SEC column was 95%, 92%, 41%, and 22% for UMRNOM, SRNOM, PPHA, and LHA, respectively, relative to the theoretical UV peak areas computed from the injected mass and UV extinction coefficients determined from the batch UV analyses (Figure 1(a)). The low recoveries for PPHA and LHA are attributed to adsorption in the SEC column (which could be visibly observed, most prominently for LHA). Regardless, the molecular weight analysis for UMRNOM, SRNOM, and PPHA shows good agreement with the UV spectral slope analysis: UMRNOM and SRNOM show very similar chromatograms with an estimated weight-average molecular weight of 20 kDa and 29 kDa, respectively, whereas PPHA shows a higher proportion of high molecular weight species with a weight-average molecular weight of 211 kDa on the portion of the sample that eluted and could be analyzed. The SEC-MALS result for the weight-average molecular weight of LHA (89 kDa) is likely severely underestimated considering the material lost on the column is likely the highest molecular weight components. Indeed, the MALS analysis for PPHA and LHA reveals that high molecular weight species showed stronger adsorptive interactions and hence eluted later than lower molecular weight species (Figure S2(b)), contrary to theoretical expectations for lower molecular weight species to elute later under ideal SEC conditions with no sample-column interactions.

3.2. Stabilization and disaggregation of lead phosphate particles by NOM in 100 mM $NaNO_3$ and 1 mM $Ca(NO_3)_2$

The lead phosphate particles showed no aggregation when diluted to 1 mg/L as Pb in the absence of any additional electrolytes, regardless of the type or concentrations of NOM added (Figure 2). All particles were highly negatively charged according to the zeta potential measurements (ζ < -30 mV, SI Figure S2), so the lack of aggregation can be consistent with electrostatic stabilization, along with possibly steric stabilization by adsorbed NOM.

In the presence of either 100 mM $NaNO_3$ (Figure 3) or 1 mM $Ca(NO_3)_2$ (Figure 4), the lead phosphate particles showed rapid aggregation without NOM but were stabilized with either 1 mg_C/L or 10 mg_C/L of NOM, which is consistent with the observation in our previous study that NOM stabilized lead phosphate particles in Ca^{2+} solution (Zhao et al., 2018). From our previous work, the CCC for lead phosphate particles in Na^+ was ≈ 69 mM (Zhao et al., 2022), and here, the measured CCC in Ca^{2+} was 0.6 mM (SI Figure S3). Hence, the NOM stabilized the particles against aggregation even in counterion concentrations higher than the CCC. NOM carries deprotonated carboxylate groups that should impart additional negative charge at pH 7, which was observed in the electrophoretic light scattering results for all types of NOM at 1 mg_C/L in either 100 mM Na^+ or 1 mM Ca^{2+}, compared to the particles in the equivalent background without NOM (Figure S1(a)). However, less negative apparent zeta potentials were observed when increasing the NOM concentrations to 10 mg_C/L (Figure S1(b)), relative to those with 1 mg_C/L of NOM. Since higher NOM concentrations should result in higher adsorbed masses that would carry more charge, the less negative apparent zeta potential is likely attributable to the fact that the measured electrophoretic mobility is influenced not only by charge but by the friction or drag on the particles (Duval and Ohshima, 2006; Hill et al., 2003; Louie et al., 2012; Ohshima, 1995). Thick or extended NOM coatings can shift the shear plane away from the particle surface and induce more significant drag forces, resulting in slower electrophoretic mobilities. This effect is not considered in the Smoluchowski model used to convert the electrophoretic mobilities of uncoated spherical particles to zeta potentials. The possibility for high molecular weight NOM coatings to result in a less negative apparent zeta potential but impart colloidal stability was similarly reported by Louie et al. (Louie et al., 2015b), and furthermore, as Romanello and Fidalgo de Cortalezzi have discussed, compression of the electrical double layer may not be the controlling mechanism for aggregation in such situations (Romanello and Fidalgo de Cortalezzi, 2013). Rather, steric or electrosteric forces are likely responsible for the particle stabilization by NOM.

Beyond the stabilization against aggregation, a further phenomenon was observed where 10 mg_C/L of NOM induced a particle size reduction compared to the initial particle diameter without NOM of (264 ± 18) nm (SI Table S4). The most significant decreases in size were induced by PPHA and LHA, with a trend of greater size reduction from ultrapure water ((170 ± 20) nm and (142 ± 7) nm for PPHA and LHA, respectively) to 100 mM $NaNO_3$ ((135 ± 8) nm and (131 ± 6) nm) to 1 mM $Ca(NO_3)_2$ ((55 ± 2) nm and (70 ± 2) nm). Control experiments were also conducted to monitor the size of 10 mg_C/L of NOM (without particles) in the different background electrolytes. UMRNOM and SRNOM did not provide sufficient light scattering to acquire reliable sizes, with mean count rates < 100 kcps (SI Table S5). However, the 10 mg_C/L solutions of PPHA and LHA produced mean count rates between 100 kcps and 400 kcps. From Figures 2(c), 3(c), and 4(c), PPHA and LHA showed a similarly drastic reduction in size from ultrapure water to 100 mM $NaNO_3$ to 1 mM $Ca(NO_3)_2$. The decrease in size of the PPHA or LHA itself in 100 mM Na^+ can be attributable to charge screening, resulting in lower intramolecular repulsion between charged moieties such as carboxylates, ~~while~~ whereas the greater size decrease in the presence of 1 mM Ca^{2+} can be attributable to charge screening and intramolecular bridging, both resulting in a denser NOM structure and smaller size.

The lead phosphate particle sizes in the presence of the PPHA and LHA were notably similar to the sizes measured for PPHA and LHA alone. Three potential reasons for the similarity in size were investigated: (1) the DLS measurements could be more sensitive to the NOM than the lead phosphate particles in the mixtures; (2) NOM could induce dissolution of the lead phosphate particles; and (3) NOM could induce particle disaggregation.

The potential measurement interference of the NOM was evaluated by comparing scattering intensities of the particles and NOM in the DLS measurements in ultrapure water, 100 mM $NaNO_3$, and 1 mM $Ca(NO_3)_2$ (SI Table S5). Count rates were similar or higher for the particles without NOM, compared to the PPHA or LHA without particles. Therefore, if the particles remain at their initial hydrodynamic size after mixing with the NOM, the contribution of the lead phosphate particles to the DLS measurements should not be completely obscured by the NOM scattering signal, so the observed size reduction is not attributable simply to a measurement interference.

To distinguish the contributions of dissolution or disagglomeration of the lead phosphate particles to the size reduction, dissolution measurements were conducted by pelleting the lead phosphate particles in 1 mM $Ca(NO_3)_2$ by centrifugation, while collecting the supernatant for ICP-MS quantification (SI Figure S4). UV-Vis measurements on the dissolved NOM in the supernatant confirmed minimal removal of NOM after centrifugation in 1 mM $Ca(NO_3)_2$ (SI Figure S5), so the supernatant should contain both dissolved and NOM-complexed lead. The supernatant lead concentration was the lowest in the absence of NOM, i.e., $(14 \pm 2)\%$ of the total lead concentration. UMRNOM and SRNOM induced additional dissolution, i.e., $(24.3 \pm 0.9)\%$ and $(25.1 \pm 1.3)\%$, respectively, and the highest concentrations of dissolved lead were observed with the higher molecular weight PPHA and LHA, i.e., $(33.0 \pm 0.5)\%$ and $(31 \pm 3)\%$, respectively. However, even considering the highest change in dissolution of $\approx 20\%$ relative to the particles without NOM, the resulting particle diameter after dissolution would be 245 nm, assuming an initial particle diameter of 264 nm and solid spherical particles. Therefore, enhanced dissolution cannot fully explain the reductions in DLS size to 55 nm and 70 nm with PPHA and LHA, respectively. Instead, the PPHA and LHA are likely inducing disagglomeration of the lead phosphate particles to smaller aggregates or primary nanoparticles. It is noted that lead phosphate nanoparticles 40 nm in diameter were observed in our prior study when the particles were precipitated at lower lead concentrations (Zhao et al., 2018).

3.3. Stabilization and bridging flocculation of lead phosphate particles by NOM in 3 mM $Ca(NO_3)_2$

Control samples of the lead phosphate particles alone showed rapid aggregation in 3 mM $Ca(NO_3)_2$ (Figure 5(a)). After the particles were mixed with lower concentrations (1 mg_C/L) of any of the four types of NOM (Figure 5(a)), as well as with 10 mg_C/L of SRNOM or UMRNOM, the particles remained colloidally stable upon adding $Ca(NO_3)_2$ (Figure 5(b)). On the other hand, although the particles were initially disaggregated to smaller sizes after premixing with 10 mg_C/L of PPHA or LHA (time zero in Figure 5(b)), rapid aggregation occurred after adding 3 mM $Ca(NO_3)_2$. Flocculation was also observed for PPHA and LHA controls (without particles) (Figure 5(c)). Kloster et al. showed that humic acid itself aggregates more rapidly with increasing Ca^{2+} (Kloster et al., 2013), and Baalousha et al. proposed that Ca^{2+} facilitated aggregation of Suwannee River humic acid by forming intra- or intermolecular bridges (Baalousha et al., 2006), with fast Ca^{2+} binding followed by slow collision and attachment of the humic acid. Here, experiments were also conducted on PPHA or LHA alone (without particles), which indeed showed homoaggregation in the presence of 3 mM Ca^{2+} (Figure 5(c)) with a CCC at ≈ 7 mM Ca^{2+} (SI Figure S3).

As the Ca^{2+} concentration here is higher than the CCC of the bare particles (SI Figure S3), the faster rate of aggregation compared to the diffusion-limited rate for the particle-only control is indicative that the destabilization by NOM is not purely by elimination of the energy barrier for particle-particle attachment. Rather, enhanced aggregation rates are typically attributed to a bridging phenomenon, e.g., as discussed by Chen et al (Chen et al., 2006). Notably, the aggregation rate (i.e., slope of hydrodynamic diameter versus time) was also higher in the mixtures of particles and PPHA or LHA, compared to the NOM-only controls, suggesting that the observed aggregation in the mixtures represents not only NOM flocculation but also heteroaggregation between the particles and the flocculating NOM. This heteroaggregation could be a result of adsorption of HA to the particles followed by bridging and/or physical entrainment of the particles in the flocculating HA.

To more precisely evaluate surface adsorption interactions, UV-Vis spectroscopy (SI Figure S5) was first attempted to compare the relative adsorption of NOM onto the particles by a solution depletion analysis, in which the remaining NOM in solution (i.e., in the supernatant after centrifugation) is compared to the total NOM added to evaluate loss by adsorption. Controls were also collected of the NOM without particles in the various water chemistries. Even when increasing the lead phosphate particle concentration to 10 mg/L as Pb to allow higher NOM removal, insufficient NOM adsorption occurred in ultrapure water, 100 mM $NaNO_3$, or 1 mM $Ca(NO_3)_2$ to be quantifiable using this method. In 3 mM $Ca(NO_3)_2$, sedimentation of PPHA and LHA was observed in both the NOM-only controls (without particles) and in the presence of the lead phosphate particles, indicating that large, dense aggregates of the HA were formed, but precluding confirmation of adsorption to the particles using this method.

Hence, *in situ* flow cell ATR-FTIR experiments were conducted, which are sensitive and selective to only the NOM adsorbing directly on the surfaces of the lead phosphate particles deposited on the ATR crystal. Figure 6 confirms adsorption of both PPHA and LHA in 3 mM $Ca(NO_3)_2$ over time, with the characteristic peaks at $\approx$ 1580 cm^{-1} and $\approx$ 1390 cm^{-1} corresponding to asymmetric and symmetric stretching, respectively, of the deprotonated carboxylate moieties (Mathew et al., 2021; Yoon et al., 2005). Control experiments on PPHA or LHA alone showed no deposition of the NOM in the *in situ* flow ATR-FTIR setup. In addition, no measurable desorption could be observed after flushing the coated particles in 3 mM $Ca(NO_3)_2$ without NOM, indicating a strong adsorptive interaction rather than physical deposition of NOM onto the particles. The PPHA and LHA adsorption were also determined to be higher in 3 mM $Ca(NO_3)_2$ than in 100 mM $NaNO_3$ (Figure 6 and SI Figure S6), with only PPHA showing detectable ATR-FTIR signals in $NaNO_3$. The UMRNOM and SRNOM showed no detectable signals in any of the media (SI Figures S6 and S7), but the colloidal stabilization of the particles in the presence of the NOM compared to without NOM in the DLS experiments implies that some adsorption must occur despite being below detection. Higher sensitivity methods, such as multi-reflection ATR-FTIR measurements, would be necessary to detect these interactions.

Finally, to investigate the floc structure of the particles with PPHA or LHA, SLS measurements were collected. A prior study by Amal et al. applied SLS to investigate the structure of large aggregates of hematite nanoparticles and observed that bridging by NOM produced lower fractal dimension aggregates that became more compact over time (Amal et al., 1990). SLS measurements were conducted here (SI Figure S8) to compare the lead phosphate particles and their aggregates in the various media without NOM, the PPHA or LHA aggregates (without lead phosphate) in 3 mM $Ca(NO_3)_2$, and the mixtures of particles and PPHA or LHA in 3 mM $Ca(NO_3)_2$. The PPHA and LHA aggregates showed scattering intensities an a order of magnitude higher than aggregates of the lead phosphate particles alone, and the SLS profiles of the mixtures of particles and HA were similar to those of the HA alone. Therefore, the SLS results likely reflect the structure of primarily the HA flocs, with the lead phosphate particles more sparsely distributed within the HA flocs.

Figure 7 summarizes the results observed across all four types of NOM at the two concentrations evaluated and the four background water chemistries. Overall, NOM imparted colloidal stabilization under all conditions, except when high molecular weight NOM (PPHA and LHA) are present at high concentrations (10 mg_C/L) and with high concentrations of Ca^{2+} (3 mM). These results suggest that a threshold in both NOM and Ca^{2+} concentrations together must be surpassed for bridging flocculation to occur. Although adsorption of PPHA and LHA to the lead phosphate particles can initially induce particle disaggregation, the addition of high Ca^{2+} causes more rapid flocculation through Ca^{2+} bridging of adsorbed NOM coatings on the particles, as well as potentially particle entrainment in the NOM flocs. Although Ca^{2+} bridging is expected to occur between carboxylate groups on the NOM, flocculation only occurred for the PPHA and LHA and did not correlate positively with the carboxyl content across the four NOM (SI Table S2). Therefore, the high molecular weight and high aromaticity of the PPHA and LHA are likely more important factors for bridging flocculation.

Conclusions

This research demonstrates that the water chemistry has a critical influence on the aggregation behavior of lead phosphate particles that form when phosphate is applied to remediate lead-contaminated environments. Highly variable outcomes (colloidal stabilization or flocculation) are possible depending on the composition and concentration of NOM and background electrolytes. In the majority of scenarios tested, including all conditions with low molecular weight aquatic NOM (e.g., SRNOM and UMRNOM), and all NOM types (SRNOM, UMRNOM, PPHA, and LHA) with 100 mM Na^{+}, low Ca^{2+} concentration (1 mM), or low NOM concentration (1 mg_C/L), the NOM imparted colloidal stability or even induced disaggregation of the lead phosphate particles. This study specifically delineated the conditions required for rapid aggregation of the particles by NOM, namely the presence of high molecular weight humic acids (e.g., PPHA or LHA) at high concentrations (10 mg_C/L) with high concentrations of Ca^{2+} (e.g., 3 mM). The self-interactions of PPHA and LHA largely explain their effects in the different Ca^{2+} concentrations, with low Ca^{2+} resulting in only intramolecular bridging of the NOM, but higher Ca^{2+} resulting in intermolecular bridging and rapid flocculation. These results suggest that a basic characterization of the NOM (molecular weight and concentration) and Ca^{2+} levels in a given water or soil can be prioritized as important predictors of lead phosphate particle aggregation and transport behavior. For soil remediation applications, the use of apatite as a phosphate source would simultaneously provide Ca^{2+}, and therefore could be an effective strategy to induce flocculation of lead phosphate particles in the presence of soil humic acids and thereby reduce their transport risk.

Acknowledgements

We thank Dr. Charisma Lattao for assistance in TOC measurements, and Chinasa Nwachukwu and Utienyin Pemu for helping with the DLS measurements. This work was supported by the National Science Foundation (NSF, Awards # 1604042, 1603717, 1705511, and 2125480).

Supporting Information Available

The supporting information includes additional NOM characterization, aggregation and adsorption results, and SLS measurements.

References

Abbt-Braun, G., Lankes, U., Frimmel, F.H., 2004. Structural characterization of aquatic humic substances - The need for a multiple method approach. Aquat. Sci. 66, 151–170. https://doi.org/10.1007/s00027-004-0711-z

Abe, T., Kobayashi, S., Kobayashi, M., 2011. Aggregation of colloidal silica particles in the presence of fulvic acid, humic acid, or alginate: Effects of ionic composition. Colloids Surfaces A Physicochem. Eng. Asp. 379, 21–26. https://doi.org/10.1016/J.COLSURFA.2010.11.052

Amal, R., Raper, J.A., Waite, T.D., 1990. Fractal structure of hematite aggregates. J. Colloid Interface Sci. 140, 158–168. https://doi.org/10.1016/0021-9797(90)90331-H

Baalousha, M., Motelica-Heino, M., Coustumer, P. Le, 2006. Conformation and size of humic substances: Effects of major cation concentration and type, pH, salinity, and residence time. Colloids Surfaces A Physicochem. Eng. Asp. 272, 48–55. https://doi.org/10.1016/J.COLSURFA.2005.07.010

Bala, T., Prasad, B.L.V., Sastry, M., Kahaly, M.U., Waghmare, U. V., 2007. Interaction of different metal ions with carboxylic acid group: A quantitative study. J. Phys. Chem. A 111, 6183–6190. https://doi.org/10.1021/jp067906x

Bricaud, A., Morel, A., Prieur, L., 1981. Absorption by dissolved organic matter of the sea (yellow substance) in the UV and visible domains. Limnol. Oceanogr. 26, 43–53. https://doi.org/10.4319/lo.1981.26.1.0043

Chen, K.L., Elimelech, M., 2007. Influence of humic acid on the aggregation kinetics of fullerene (C60) nanoparticles in monovalent and divalent electrolyte solutions. J. Colloid Interface Sci. 309, 126–134. https://doi.org/10.1016/J.JCIS.2007.01.074

Chen, K.L., Mylon, S.E., Elimelech, M., 2006. Aggregation Kinetics of Alginate-Coated Hematite Nanoparticles in Monovalent and Divalent Electrolytes. Environ. Sci. Technol. 40, 1516–1523. https://doi.org/10.1021/es0518068

Chin, Y.P., Alken, G., O'Loughlin, E., 1994. Molecular Weight, Polydispersity, and Spectroscopic Properties of Aquatic Humic Substances. Environ. Sci. Technol. 28, 1853–1858. https://doi.org/10.1021/es00060a015

Deonarine, A., Hsu-Kim, H., 2009. Precipitation of mercuric sulfide nanoparticles in NOM-containing water: Implications for the natural environment. Environ. Sci. Technol. 43, 2368–2373. https://doi.org/10.1021/es803130h

Deonarine, A., Lau, B.L.T., Aiken, G.R., Ryan, J.N., Hsu-Kim, H., 2011. Effects of humic substances on precipitation and aggregation of zinc sulfide nanoparticles. Environ. Sci. Technol. 45, 3217–3223. https://doi.org/10.1021/es1029798

Deshommes, E., Trueman, B., Douglas, I., Huggins, D., Laroche, L., Swertfeger, J., Spielmacher, A., Gagnon, G.A., Prévost, M., 2018. Lead Levels at the Tap and Consumer Exposure from Legacy and Recent Lead Service Line Replacements in Six Utilities. Environ. Sci. Technol. 52, 9451–9459. https://doi.org/10.1021/acs.est.8b02388

Duval, J.F.L., Ohshima, H., 2006. Electrophoresis of diffuse soft particles. Langmuir 22, 3533–3546. https://doi.org/10.1021/la0528293

Ghosh, S., Mashayekhi, H., Pan, B., Bhowmik, P., Xing, B., 2008. Colloidal behavior of aluminum oxide nanoparticles as affected by pH and natural organic matter. Langmuir 24, 12385–12391. https://doi.org/10.1021/LA802015F/ASSET/IMAGES/LARGE/LA-2008-02015F_0009.JPEG

Guo, C., Tian, W., Wang, Z., Han, F., Su, M., Wu, Y., Li, Z., Hu, S., 2019. Reduction of Pb availability during surficial leaching in different types of soils with addition of apatite and oxalic acid. J. Soils Sediments 19, 741–749. https://doi.org/10.1007/s11368-018-2100-6

Hanna-Attisha, M., LaChance, J., Sadler, R.C., Champney Schnepp, A., 2016. Elevated Blood Lead Levels in Children Associated With the Flint Drinking Water Crisis: A Spatial Analysis of Risk and Public Health Response. Am. J. Public Health 106, 283–90. https://doi.org/10.2105/AJPH.2015.303003

Hill, R.J., Saville, D.A., Russel, W.B., 2003. Electrophoresis of spherical polymer-coated colloidal particles. J. Colloid Interface Sci. 258, 56–74. https://doi.org/10.1016/S0021-9797(02)00043-7

Huangfu, X., Jiang, J., Ma, J., Liu, Y., Yang, J., 2013. Aggregation Kinetics of Manganese Dioxide Colloids in Aqueous Solution: Influence of Humic Substances and Biomacromolecules. Environ. Sci. Technol. 47, 10285–10292. https://doi.org/10.1021/ES4003247

International Humic Substances Society (IHSS), 2022. IHSS | International Humic Substances Society [WWW Document]. URL http://humic-substances.org/#products (accessed 1.7.21).

Jalilehvand, F., Sisombath, N.S., Schell, A.C., Facey, G.A., 2015. Lead(II) complex formation with L-cysteine in aqueous solution. Inorg. Chem. 54, 2160–2170. https://doi.org/10.1021/ic5025668

Kloster, N., Brigante, M., Zanini, G., Avena, M., 2013. Aggregation kinetics of humic acids in the presence of calcium ions. Colloids Surfaces A Physicochem. Eng. Asp. 427, 76–82. https://doi.org/10.1016/J.COLSURFA.2013.03.030

Landrot, G., Khaokaew, S., 2018. Lead Speciation and Association with Organic Matter in Various Particle-Size Fractions of Contaminated Soils. Environ. Sci. Technol. 52, 6780–

6788. https://doi.org/10.1021/acs.est.8b00004

Liu, X., Wazne, M., Chou, T., Xiao, R., Xu, S., 2011. Influence of Ca2+ and Suwannee River Humic Acid on aggregation of silicon nanoparticles in aqueous media. Water Res. 45, 105–112. https://doi.org/10.1016/J.WATRES.2010.08.022

Louie, S.M., Phenrat, T., Small, M.J., Tilton, R.D., Lowry, G. V., 2012. Parameter identifiability in application of soft particle electrokinetic theory to determine polymer and polyelectrolyte coating thicknesses on colloids. Langmuir 28, 10334–10347. https://doi.org/10.1021/la301912j

Louie, S.M., Spielman-Sun, E.R., Small, M.J., Tilton, R.D., Lowry, G. V., 2015a. Correlation of the physicochemical properties of natural organic matter samples from different sources to their effects on gold nanoparticle aggregation in monovalent electrolyte. Environ. Sci. Technol. 49, 2188–2198. https://doi.org/10.1021/es505003d

Louie, S.M., Spielman-Sun, E.R., Small, M.J., Tilton, R.D., Lowry, G. V., 2015b. Correlation of the physicochemical properties of natural organic matter samples from different sources to their effects on gold nanoparticle aggregation in monovalent electrolyte. Environ. Sci. Technol. 49, 2188–2198. https://doi.org/10.1021/es505003d

Louie, S.M., Tilton, R.D., Lowry, G. V., 2013. Effects of Molecular Weight Distribution and Chemical Properties of Natural Organic Matter on Gold Nanoparticle Aggregation. Environ. Sci. Technol. 47, 4245–4254. https://doi.org/10.1021/es400137x

Ma, Q.Y., Traina, S.J., Logan, T.J., Ryan, J.A., 1993. In Situ Lead Immobilization by Apatite. Environ. Sci. Technol. 27, 1803–1810. https://doi.org/10.1021/es00046a007

Mathew, R.A., Wu, G., Zhang, Y., Shakiba, S., Yao, Y., Tsai, A.L., Louie, S.M., 2021. Natural organic matter adsorption conditions influence photocatalytic reaction pathways of phosphate-treated titanium dioxide nanoparticles. Environ. Sci. Nano 8, 2165–2176. https://doi.org/10.1039/D1EN00433F

Mavropoulos, E., Rossi, A.M., Costa, A.M., Perez, C.A.C., Moreira, J.C., Saldanha, M., 2002. Studies on the mechanisms of lead immobilization by hydroxyapatite. Environ. Sci. Technol. 36, 1625–1629. https://doi.org/10.1021/es0155938

Ohshima, H., 1995. Electrophoresis of soft particles. Adv. Colloid Interface Sci. 62, 189–235. https://doi.org/10.1016/0001-8686(95)00279-Y

Romanello, M.B., Fidalgo de Cortalezzi, M.M., 2013. An experimental study on the aggregation of TiO2 nanoparticles under environmentally relevant conditions. Water Res. 47, 3887–3898. https://doi.org/10.1016/j.watres.2012.11.061

Ruby, M. V., Davis, A., Nicholson, A., 1994. In Situ Formation of Lead Phosphates in Soils as a Method to Immobilize Lead. Environ. Sci. Technol. 28, 646–654. https://doi.org/10.1021/es00053a018

Shakiba, S., Hakimian, A., Barco, L.R., Louie, S.M., 2018. Dynamic Intermolecular Interactions Control Adsorption from Mixtures of Natural Organic Matter and Protein onto Titanium Dioxide Nanoparticles. Environ. Sci. Technol. 52, 14158–14165. https://doi.org/10.1021/acs.est.8b04014

Shen, M.H., Yin, Y.G., Booth, A., Liu, J.F., 2015. Effects of molecular weight-dependent physicochemical heterogeneity of natural organic matter on the aggregation of fullerene nanoparticles in mono- and di-valent electrolyte solutions. Water Res. 71, 11–20. https://doi.org/10.1016/J.WATRES.2014.12.025

Thurman, E.M., 1985. Organic Geochemistry of Natural Waters. Springer Netherlands. https://doi.org/10.1007/978-94-009-5095-5

Tiller, C.L., O’Melia, C.R., 1993. Natural organic matter and colloidal stability: Models and measurements. Colloids Surfaces A Physicochem. Eng. Asp. 73, 89–102. https://doi.org/10.1016/0927-7757(93)80009-4

Vindedahl, A.M., Stemig, M.S., Arnold, W.A., Penn, R.L., 2016. Character of Humic Substances as a Predictor for Goethite Nanoparticle Reactivity and Aggregation. Environ. Sci. Technol. 50, 1200–1208. https://doi.org/10.1021/ACS.EST.5B04136/ASSET/IMAGES/LARGE/ES-2015-041366_0005.JPEG

Wei, W., Cui, J., Wei, Z., 2014. Effects of low molecular weight organic acids on the immobilization of aqueous Pb(II) using phosphate rock and different crystallized hydroxyapatite. Chemosphere 105, 14–23. https://doi.org/10.1016/j.chemosphere.2013.09.121

Wu, Y., Lou, J., Sun, X., Ma, L.Q., Wang, J., Li, M., Sun, H., Li, H., Huang, L., 2020. Linking elevated blood lead level in urban school-aged children with bioaccessible lead in neighborhood soil. Environ. Pollut. 261, 114093. https://doi.org/10.1016/j.envpol.2020.114093

Yoon, T.H., Johnson, S.B., Brown, G.E., 2005. Adsorption of Organic Matter at Mineral/Water Interfaces. IV. Adsorption of Humic Substances at Boehmite/Water Interfaces and Impact on Boehmite Dissolution. Langmuir 21, 5002–5012. https://doi.org/10.1021/la0476276

Zhang, X., Yang, L., Li, Y., Li, H., Wang, W., Ye, B., 2012. Impacts of lead/zinc mining and smelting on the environment and human health in China. Environ. Monit. Assess. 184, 2261–2273. https://doi.org/10.1007/s10661-011-2115-6

Zhao, J., Giammar, D.E., Pasteris, J.D., Dai, C., Bae, Y., Hu, Y., 2018. Formation and Aggregation of Lead Phosphate Particles: Implications for Lead Immobilization in Water

Supply Systems. Environ. Sci. Technol. 52, 12612–12623. https://doi.org/10.1021/acs.est.8b02788

Zhao, J., Mowla, M., Pan, Z., Bao, D., Giammar, D.E., Hu, Y., Louie, S.M., 2022. Lead phosphate deposition in porous media and implications for lead remediation. Water Res. 214, 118200. https://doi.org/10.1016/J.WATRES.2022.118200

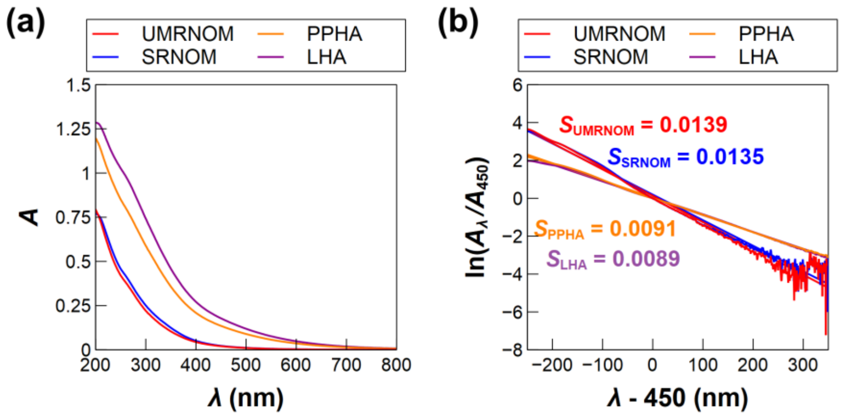

Figure 1. UV-Vis absorbance spectra (a) and fitted exponential slopes, *S* (b), for solutions of 10 mg_C/L of UMRNOM, SRNOM, PPHA, and LHA at pH 7.

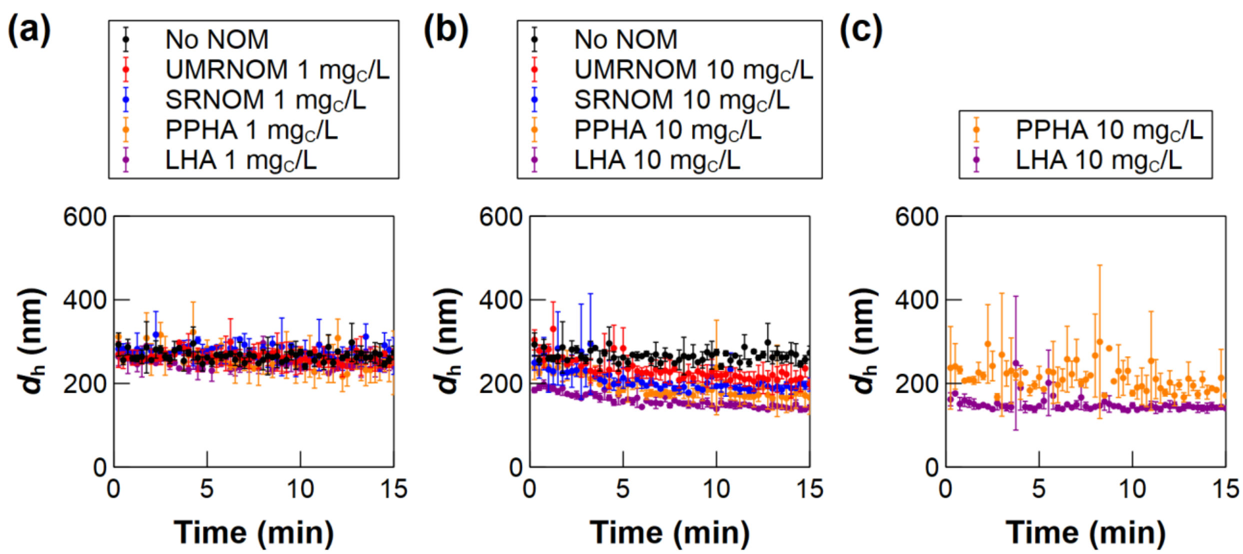

Figure 2. Size evolution of lead phosphate particles in ultrapure water without NOM or with 1 mg_C/L (a) or 10 mg_C/L (b) of NOM, and (c) size evolution of 10 mg_C/L of PPHA or LHA in ultrapure water.

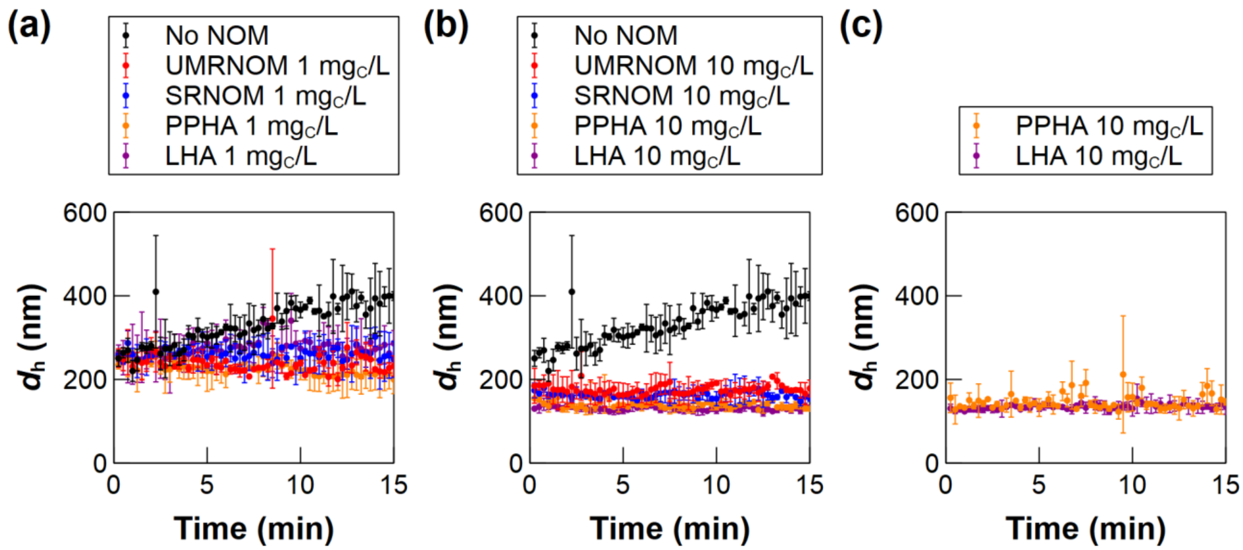

Figure 3. Size evolution of lead phosphate particles in 100 mM $NaNO_3$ without NOM or with 1 mg_C/L (a) or 10 mg_C/L (b) of NOM, and (c) size evolution of 10 mg_C/L of PPHA or LHA in 100 mM $NaNO_3$.

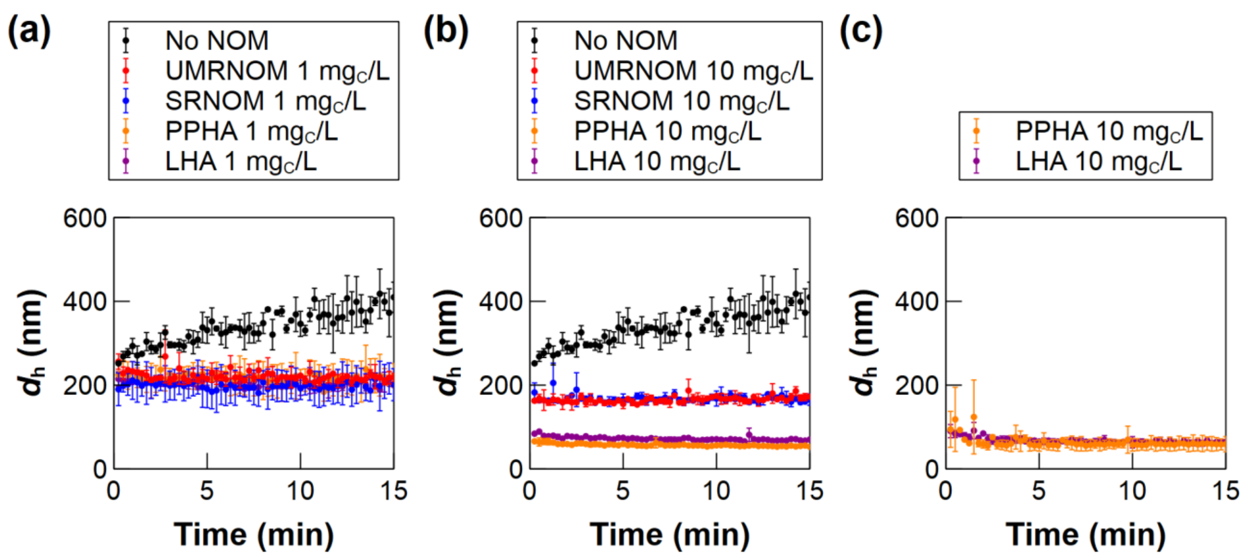

Figure 4. Size evolution of lead phosphate particles in 1 mM $Ca(NO_3)_2$ without NOM or with 1 mg_C/L (a) or 10 mg_C/L (b) of NOM, and (c) size evolution of 10 mg_C/L of PPHA or LHA in 1 mM $Ca(NO_3)_2$.

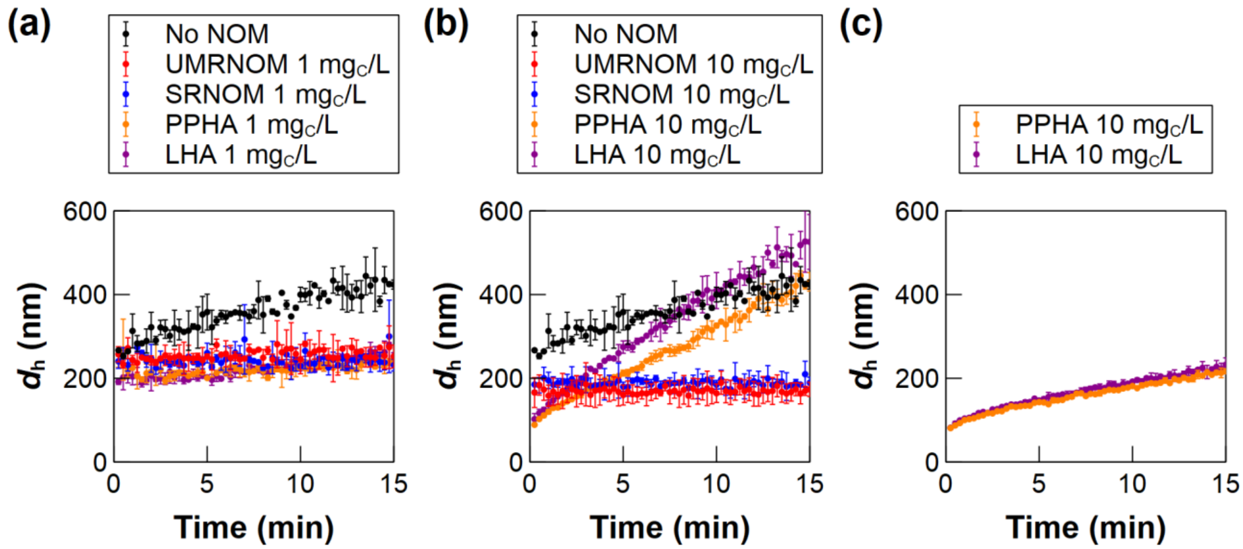

Figure 5. Size evolution of lead phosphate particles in 3 mM $Ca(NO_3)_2$ without NOM or with 1 mg$_C$/L (a) or 10 mg$_C$/L (b) of NOM, and (c) size evolution of 10 mg$_C$/L of PPHA or LHA in 3 mM $Ca(NO_3)_2$.

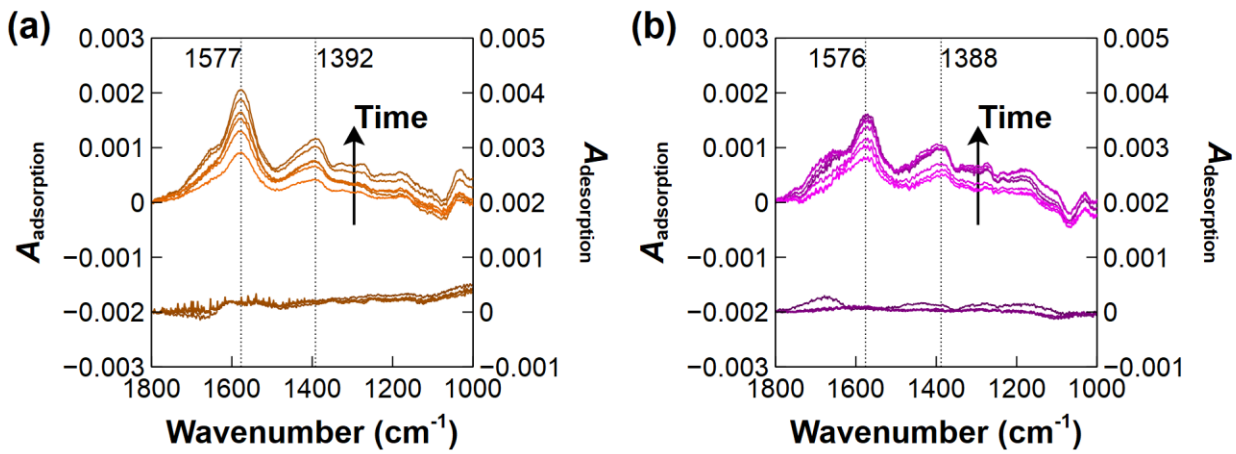

Figure 6. *In situ* ATR-FTIR analysis of the interactions of PPHA (a) and LHA (b) with lead phosphate particles in 3 mM $Ca(NO_3)_2$. After equilibrating in 3 mM $Ca(NO_3)_2$ without NOM, adsorption was monitored in 5 min intervals up to 35 min from NOM solutions at 10 mg_C/L (top series in each plot), with the last spectrum collected in 3 mM $Ca(NO_3)_2$ used for background subtraction from the adsorption spectra. Desorption was evaluated in 5 min intervals up to 15 min (bottom series in each plot), with the last spectrum collected from the adsorption phase used for background spectra from the desorption spectra.

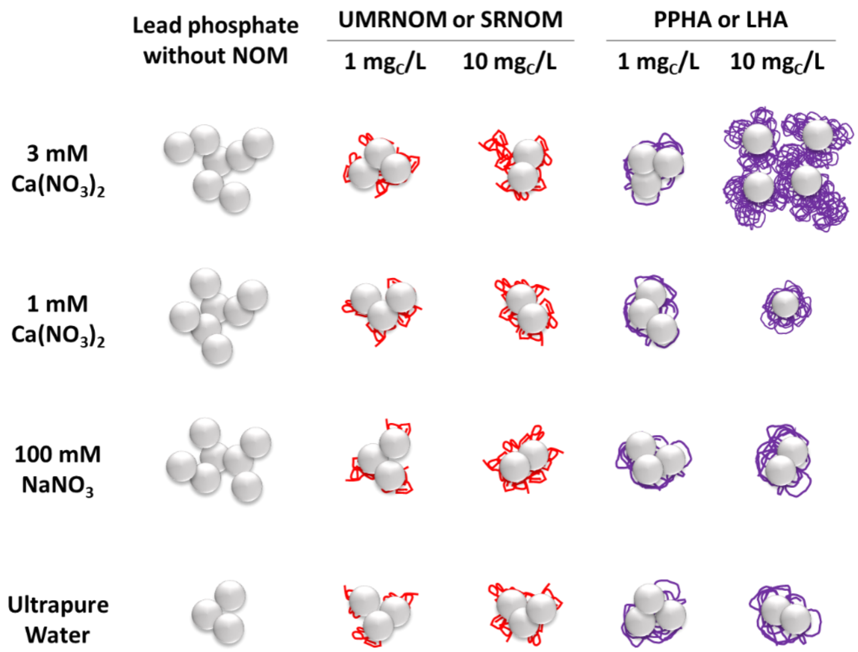

Figure 7. Summary of lead phosphate particle stabilization, disaggregation, and flocculation observed depending on the compositions and concentrations of NOM and background electrolytes.

TOC Art

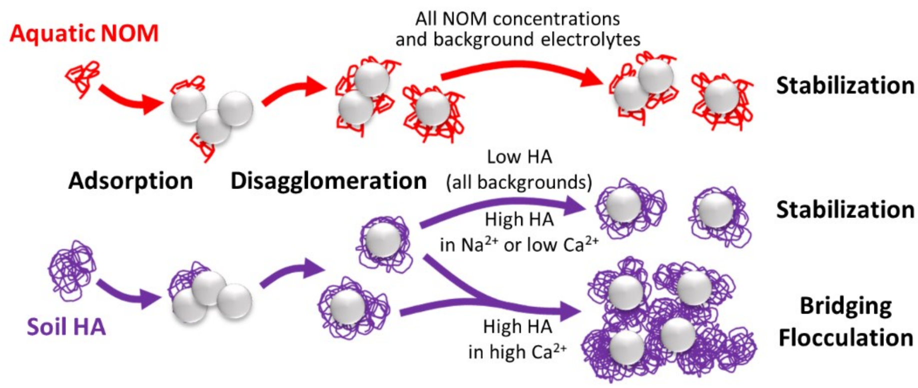

Aquatic NOM
All NOM concentrations
and background electrolytes
Stabilization
Adsorption
Disagglomeration
Low HA
(all backgrounds)
Stabilization
High HA
in Na^{2+} or low Ca^{2+}
Soil HA
High HA
in high Ca^{2+}
Bridging
Flocculation